Physics Letters A 384 (2020) 126789

Contents lists available at ScienceDirect

Physics Letters A

www.elsevier.com/locate/pla

Structural, electronic and thermoelectric properties of topological semimetal lanthanum monopnicitide LaBi

Nisha [a], Hardev S. Saini [a,*], Narender Kumar [a,b], Satyender Singhmar [a], Jyoti Thakur [a], Sunita Srivastava [a,c], Manish K. Kashyap [d], Ali H. Reshak [e,f,g]

[a] Department of Physics, Guru Jambheshwar University of Science & Technology, Hisar-125001, Haryana, India
[b] Dayanand College, Hisar-125001, Haryana, India
[c] Department of Physics, Panjab University, Chandigarh-160014, India
[d] Department of Physics, Kurukshetra University, Kurukshetra-136119, Haryana, India
[e] Physics Department, College of Science, Basrah University, Basrah, Iraq
[f] Department of Instrumentation and Control Engineering, Faculty of Mechanical Engineering, CTU in Prague, Technicka 4, Prague 6 166 07, Czech Republic
[g] Nanotechnology and Catalysis Research Center (NANOCAT), University of Malaya, Kuala Lumpur, 50603, Malaysia

ARTICLE INFO

Article history:
Received 17 April 2020
Received in revised form 11 July 2020
Accepted 2 August 2020
Available online 11 August 2020
Communicated by L. Ghivelder

Keywords:
Transport properties
DFT
FPLAPW method
Boltzmann transport theory
Topological Semimetal

ABSTRACT

The structural, electronic and thermoelectric properties of LaBi have been studied using density functional theory (DFT) combined with semiclassical Boltzmann transport theory. The exchange and correlation (XC) effects have been treated using local density approximation (LDA) including spin-orbit coupling (SOC). In the present work, we have determined the topological character of LaBi, which is in agreement with available theoretical and experimental studies. The elastic constants such as Bulk modulus, Young modulus, Poisson's ratio and shear anisotropy factor have been calculated to check the mechanical stability. The thermoelectric transport parameters such as Seebeck coefficient, Power factor, electrical and thermal conductivity are calculated as a function of temperature and chemical potential. The values of power factor and lattice thermal conductivity are found to be 1.34×10^{13} $WK^{-2}m^{-1}sec^{-1}$ and 4.20 $Wm^{-1}K^{-1}$, respectively, at T =1000 K. The calculated value of figure of merit ZT is 0.42 at T =1000 K, suggesting that LaBi may be used as an effective thermoelectric material for high temperature applications.

1. Introduction

As energy crisis is one of the biggest challenges for the mankind, and hence consequently by improving the alternate energy resources would help fulfill the increasing demands of energy. The Thermoelectric (TE) materials provide environmental-friendly solution for the conversion of heat to electricity and vice-versa [1,2]. They are useful in many significant applications such as power generation, refrigeration and energy saving etc. One of the important parameters, which decide the performance of TE materials, is termed as dimensionless figure of merit (ZT) which is defined as:

$$ZT = \frac{\sigma S^2 T}{k_e + k_l} \quad (1)$$

where S, σ, T, k_e and k_l are Seebeck coefficient, electrical conductivity, absolute temperature, electronic and lattice part of thermal conductivity, respectively. $S^2\sigma$ is known as power factor (PF). The efficiency of TE materials can be improved by increasing the dimensionless figure of merit (ZT), this is possible with large value of power factor (PF) and small value of total thermal conductivity. But improving ZT is a big challenge as it is a combination of conflicting physical quantities which are coupled with each other [3].

Many materials such as Skutterudites, Clathrates, transition metal Chalcogenides, half/full Heusler alloys and Topological insulators (TIs) have been used as thermoelectric materials from last two decades over a wide range of temperature [4–9]. Among them, TIs are excellent thermoelectric materials for which large thermoelectric efficiencies have been reported by many theoretical and experimental groups [10–12]. The bulk electronic band structure of TI behaves as ordinary band insulator, but they have gapless surface states at the boundary [13,14]. The TIs are potentially excellent thermoelectric materials due to two main reasons; (i) they possess narrow band gap associated with band inversion, which is also favorable for optimization of thermoelectric performance

* Corresponding author.
E-mail addresses: hardevdft@gmail.com, hardev1984@gjust.org (H.S. Saini).

https://doi.org/10.1016/j.physleta.2020.126789
0375-9601/

and (ii) they are generally consist of heavy atoms having large atomic mass which is helpful in maintaining low lattice thermal conductivity [15,16]. The charge transport in these materials is dissipationless or the backscattering is suppressed, which is crucial for high thermoelectric performance [17]. In present scenario, the research has been extended from TIs to Topological semimetals (TSMs) [18], where the surface states possess high carrier mobilities and large value of magnetoresistance [19]. Based on various experimental and theoretical data, TSMs are classified into three types: Weyl, Dirac, and nodal line semimetals [20–22]. The transformation of topological semimetals from one form into another by breaking one or more sets of symmetries makes their study more important [23].

Recently, the family of Rare-earth monopnictides with La in a rock salt crystal structure such as LaX (X= P, As, Sb and Bi) have drawn special attentions due to their extreme magnetoresistances and possible topological states [24–26]. Several theoretical and experimental reports have confirmed that LaBi exhibits large magnetoresistance, high carrier mobility and huge bulk conductivity [25,27,28]. The high melting point, extreme hardness, and mechanical strength make LaBi a promising technological material for different applications such as hard coatings and magnetic storage devices [29].

Nayak et al. [30] investigated the topological surface states of LaBi using angle resolved photoemission spectroscopy (ARPES) and revealed the existence of surface states of LaBi by observation of three dirac cones: one appears at the center of Brillouin zone and two coexisting at the corners. They also performed the band-structure calculations based on density functional theory (DFT) and confirmed the topological surface state of LaBi. Lou et al. [31] investigated the electronic structure and topological characteristics of LaBi using ARPES and found that LaBi exhibits band inversion along Γ-X direction, having presence of one massless and one gapped Dirac like surface state at X and Γ, respectively. They identified odd number of Dirac cones which strongly suggests non-trivial band topology of LaBi. Further, they performed the first-principles calculations including spin-orbit coupling to investigate the bulk electronic band structure and confirmed the non-trivial band anticrossing along Γ-X direction in LaBi. Niu et al. [32] studied the presence of electronic surface states in LaBi using ARPES experiment and found odd number of Dirac cone present below the Fermi level at the (001) surface. They also identified the band anticrossing along Γ-X direction in LaBi. Recently, Feng et al. [33] observed node-line-like surface states in LaBi using angle-resolved photoemission spectroscopy, which is beneficial in understanding large magnetoresistance.

Theoretically, Dey et al. [34] performed the *ab-initio* calculations of bulk and surface band structures of LaBi, LaSb and their multilayer using full potential linearlized augmented plane wave (FPLAPW) method. They calculated Z_2 invariant from bulk and surface bandstructure, which confirms the topologically non-trivial Z_2 semi-metal character of LaBi. Further, they found that the shape or nature of the Dirac cone is unaffected by uniaxial strain on the (001) surface of LaBi. The electronic structures of LaBi and LuBi using FPLAPW method were investigated by Dey [35]. She proved that LaBi behaves as Z_2 topological semimetal. She also performed the surface state calculations on (001) and (111) surfaces and showed the presence of single Dirac cone. Recently, Zhou et al. [36] calculated the thermoelectric properties of similar topological insulator LaP using first-principles calculations together with Boltzmann transport theory and confirmed the dynamical stability of material by phonon dispersion having no imaginary modes. They also examined ZT from temperature range 300 to 700 K and found its value as 0.36 for carrier concentration $n = 10^{20}$ cm^{-3} (T =700 K) which suggests that LaP may be a potential thermoelectric material. Apart from La monopnicitides, several first-principles calculations along with semiclassical Boltzmann transport theory on various TSMs such as ZrTe [37], TaAs [38], Cd_3As_2 [39], NbP [40], MoP [41] etc. were performed to investigate the effect of their topological characters in enhancing the thermoelectric properties.

On reviewing the literature, we found that the TSMs enhance the efficiency of thermoelectric devices due to their large electrical conductivities and low lattice thermal conductivities. In the present work, we plan to perform first principles calculations to study the structural, electronic and thermoelectric properties of LaBi with an aim to justify its candidature for futuristic thermoelectric devices via detailed investigation.

2. Computational details

The first principles simulations were performed to calculate the structural, electronic and thermoelectric properties of LaBi using the full-potential linearized augmented plane wave (FPLAPW) method as implemented in WIEN2k code [42]. For exchange-correlation (XC) potential, the local density approximation (LDA) and modified Becke Johnson (mBJ) potential with and without spin-orbit coupling (SOC) was used. The calculation of structural properties using LDA for heavier elements yield the values closer to experimental values as compared to that using Generalized gradient approximation (GGA) [43] and modified Becke and Johnson (mBJ) potential. This is the main reason for selecting LDA to report transport properties. The cut off energy, $E = -6.0$ Ry, defining the separation between the core and valence states, was used in all calculations. The value of $R_{MT} \times K_{max} = 7$ was setup where K_{max} is the largest k-vector used in the plane-wave expansion and R_{MT} denotes the smallest atomic sphere radius. For the calculation of elastic constants, IRelast method [44], implemented in WIEN2k code was used. The transport properties of this material were calculated by combining the first-principles calculations and semiclassical Boltzmann transport theory within the constant relaxation time approximation, implemented in BoltzTraP code [45]. This semi-classical Boltzmann transport theory can provide the reliable results for the transport properties. A denser mesh of $(42\times42\times42)$ k-points was used for the calculation of TE transport properties. GIBBS code [46] was used to predict Debye temperature, which was further used for the calculation of lattice thermal conductivity. Phonopy software [47] was employed for analyzing phonon dispersion spectra based upon the framework of density-functional perturbation theory (DFPT) [48].

3. Results with discussion

3.1. Structural and electronic properties

The LaBi crystallizes into a face-centred cubic structure having space group symmetry Fm-3m (No. 225), in which La atom is positioned at (0.5, 0.5, 0.5) and Bi atom at (0, 0, 0), as shown in Fig. 1(a). The lattice parameter of the LaBi was optimized in the neighborhood of the experimental lattice parameter (6.58 Å) [34], is listed in Table 1 for various XC potentials. The structural optimization of LaBi compound is shown in Fig. 1(b).

The values of optimized lattice constant and Bulk modulus calculated from LDA in comparison to GGA functional are in good agreement with the experimental values [49] as shown in Table 1.

The energy band structures of LaBi along high symmetry directions using LDA, LDA+SOC and mBJLDA+SOC are depicted in Fig. 2. The band structure of LaBi using LDA functional reveals that there is no band inversion near high symmetry point X, both conduction band (CB) and valence band (VB) merge with each other near high symmetry point X (Fig. 2(a)). When the SOC effect is included, the

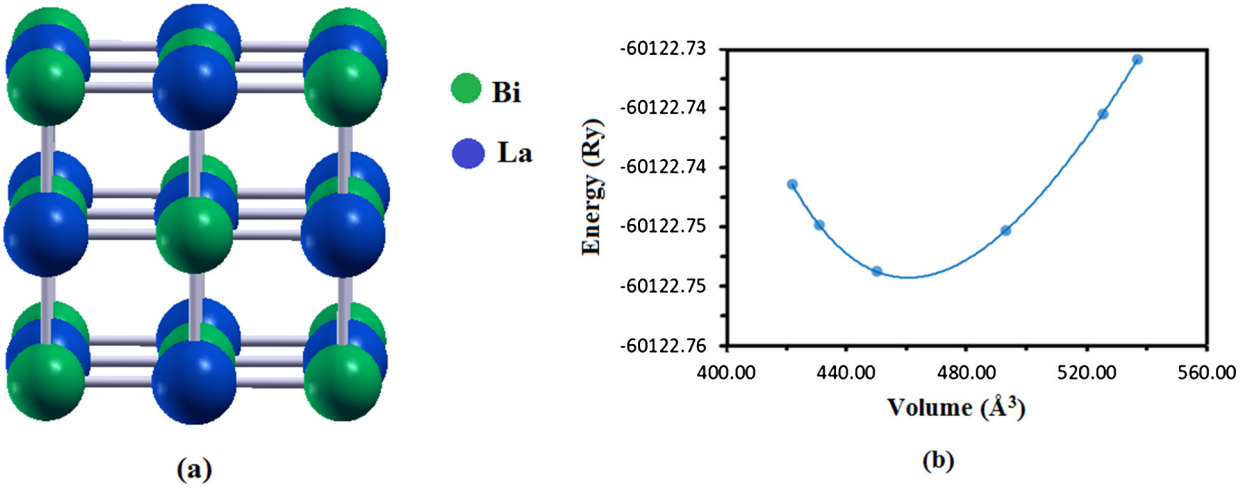

Fig. 1. (a) The FCC unit cell of LaBi and (b) Energy vs volume curve for it, as obtained from LDA calculation.

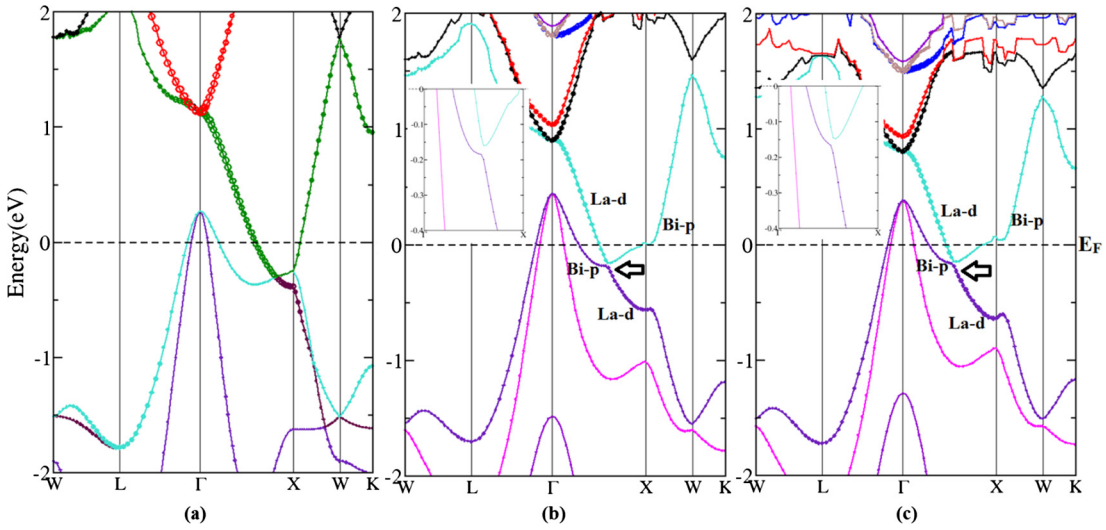

Fig. 2. Band Structure plot of LaBi using (a) LDA, (b) LDA+SOC and (c) mBJLDA+SOC approaches. The electronic gap is depicted by pointing an arrow mark and also shown with enlarged view in inset.

Table 1
Calculated Equilibrium lattice constant (Å), Bulk modulus (GPa) of LaBi compound using both GGA and LDA approaches.

Potential	Lattice constant (Å)	Bulk modulus (GPa)
LDA (This work)	6.49	58.60
GGA (This work)	6.65	43.92
Expt. Value	6.58[a]	55.0[a]

[a] Ref. [49].

significant changes in the band structure near E_F was observed as shown in Fig. 2(b).

It is clear from this figure that the CB and VB give rise to band inversion between the Γ and X points and the orbital character of band changes near the X-point which confirms the topological character of LaBi as reported by other studies [34,35]. Even parity La-5d and odd parity Bi-6p orbitals contribute to this band-inversion. The energy gap at the point of inversion (near X point) between CB and VB is about ∼21 meV, which agrees well with the available theoretical data ∼19 meV [35].

We have also calculated the band structure using mBJLDA functional to confirm the topological character of resultant compound LaBi as shown in Fig. 2(c). With the mBJLDA, the conduction band minima (CBM) near the X-point is shifted upward and the valence band maxima (VBM) at the gamma point is pushed downward, it indicates that band inversion is still there but it is consolidated by increasing the band overlap. Using mBJLDA this gap between conduction and valence band is ∼17 meV. This band inversion gap is clearly visible in the inset picture of Fig. 2(b). The corresponding total density of states (DOS) of LaBi have been plotted in Fig. 3 only using LDA and LDA+SOC functionals. We can see from the Fig that the VBM and CBM (i.e. near E_F) are mainly contributed by the La-d and Bi-p states. As SOC effect is included, the total DOS increases in the conduction band region, which is beneficial for enhancing figure of merit of LaBi.

3.2. Mechanical and thermodynamic properties

The elastic properties give information about the type of bonding between adjacent atomic planes, stiffness of material, mechanical stability and anisotropic character of bonding [50]. A Born-Huang stability criterion [51], which was used to check the stability of the material for cubic system, is given as:

$$C_{11} - C_{12} > 0, \quad C_{11} > 0, \quad C_{44} > 0 \quad \text{and} \quad C_{11} + 2C_{12} > 0 \qquad (2)$$

Our predicted values of elastic constants (Table 2) indicate that LaBi satisfies the above conditions (Eqn. (2)) and is therefore governed as mechanically stable. The values of elastic constants such

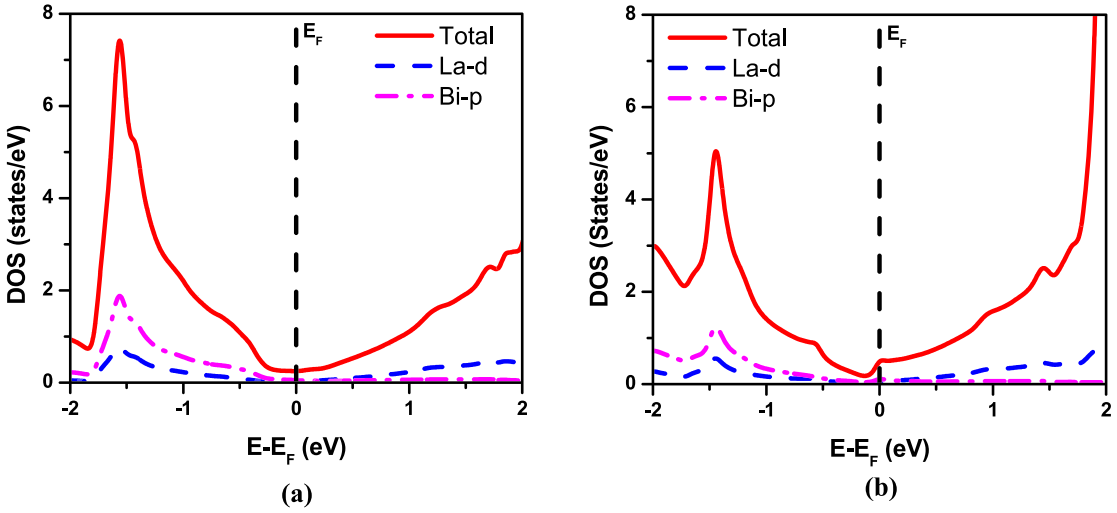

Fig. 3. Calculated Density of states (DOS) plot of LaBi using (a) LDA and (b) LDA+SOC. E_F is shifted to 0 eV.

Table 2
Calculated elastic constants of LaBi compound.

Properties	Calculated value (in GPa)	Properties	Calculated values
C_{11}	165.76	Shear elastic anisotropy (A)	0.10
C_{12}	5.03	Poisson's ratio (v)	0.33
C_{44}	5.95	Pugh's Ratio (B/G)	2.59
C_{11}–C_{12}	160.79	Frantsevich's Ratio (G/B)	0.38
C_{11}+2C_{12}	175.82	Debye Temperature (θ_D)	208.35
B (Bulk modulus)	58.59	Grüneisen Parameter (γ)	1.97
G (Shear modulus)	22.59		
Y (Young's modulus)	60.04		

as Shear elastic anisotropy (A), bulk modulus (B) and shear modulus (G) were calculated by the following relations:

$$A = \frac{2C_{44}}{C_{11} - C_{12}} \tag{3}$$

$$B = \frac{C_{11+}2C_{12}}{3} \tag{4}$$

$$G = \frac{G_{R+}G_V}{2} \tag{5}$$

whereas, $G_R = \frac{5(C_{11-C_{12}})C_{44}}{4C_{44}+3(C_{11}-C_{12})}$ and $G_V = \frac{C_{11}-C_{12+}3C_{44}}{5}$ are the Reuss [52] and Voigt [53] shear modulus, respectively.

The constants A, B and G tell about the anisotropic nature and strength of the resultant material. Again, we can estimate the Young modulus (Y) and Poisson's ratio (v) from the calculated value of bulk modulus (B) and shear modulus (G) using following relation:

$$v = \frac{(3B - 2G)}{2(3B + G)} \tag{6}$$

$$Y = \frac{9BG}{3B + G} \tag{7}$$

The parameters Y and v show the stiffness and expansion nature of interatomic forces of this compound [54–56]. The calculated elastic constants along with elastic properties such as Bulk modulus (B), Young modulus (Y), Shear modulus (G), Shear elastic anisotropy (A), Poisson's ratio (v) are listed in Table 2. The constants A, B and G tell about the anisotropic nature and strength of resultant material. The calculated value of Pugh's ratio (B/G) was found to be 2.59 which is > 1.75, which also confirms that the given material is ductile in nature [57]. Frantsevich's ratio (G/B) is equal to $\sim$0.39 which is < 1.06, thus, this material shows less resistance against shear deformation [58].

Phonon dispersion spectrum and phonon density of states (PDOS) for LaBi are depicted in Fig. 4. For this spectrum, a $2 \times 2 \times 2$ supercell was constructed with 64 atoms having displacement amplitude 0.03 Å using Phonopy code. The obtained range of phonon frequency is from 0 to 4 THz as shown in Fig. 4(a) and there is not any existence of negative frequencies for LaBi in the Brillouin zone which confirms its thermodynamic stability. The mass difference between La and Bi atoms affects the shape of phonon dispersion spectrum. On checking partial DOS (Fig. 4(b)), we observe that La and Bi atoms contribute almost equally for generation of phonon frequencies in the entire range (0–4 THz). However, for acoustic phonons with lower frequency/optical phonons having higher frequency, the contribution from Bi/La dominates slightly over the other. This spectrum has the similar shape as that for other lanthanum monopnicitides such as LaP and LaAs [59].

3.3. Thermoelectric properties

Various thermoelectric properties have been calculated using BoltzTraP code under constant relaxation time (τ) approximation. At different temperatures from 200–1000 K, the chemical potential dependence of transport coefficients such as Seebeck coefficient (S), electrical conductivity (σ/τ), electronic part of thermal conductivity (k_e/τ) and power factor (PF) (where τ is the relaxation time) were analyzed in Fig. 5(a)–(d).

The value of the chemical potential (μ) ranges from -1.5 eV to 1.5 eV for all these parameters and the negative trends of the curves i.e. from -1.5 to 0 eV show that the behavior of LaBi is p-type thermoelectric material whereas, in the range, 0 to 1.5 eV, it has n-type carriers. As shown from Fig. 5, the Seebeck coefficient, electrical conductivity and electronic part of thermal conductivity have maximum values -62.43 μVK^{-1}, 4.51×10^{22} $S\,m^{-1}sec^{-1}$ and 0.9×10^{16} $Wm^{-1}K^{-1}sec^{-1}$, respectively. These values lie in the range 0 to 1.5 eV of the chemical potential and show that the

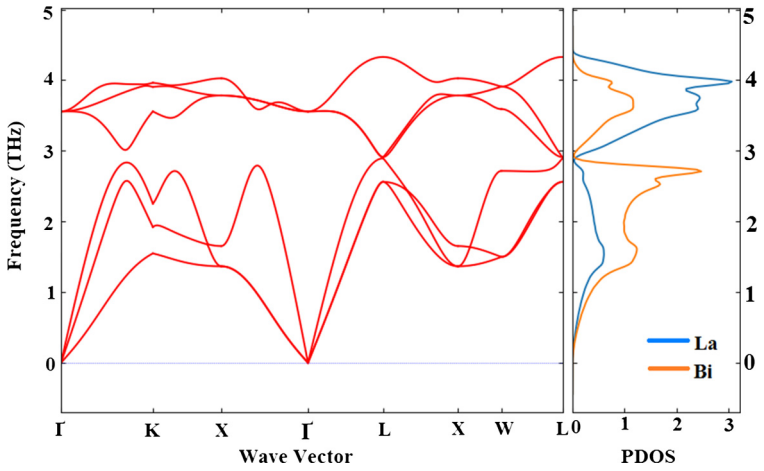

Fig. 4. (a) Phonon-dispersion spectra and (b) atom resolved density of states (DOS) of LaBi.

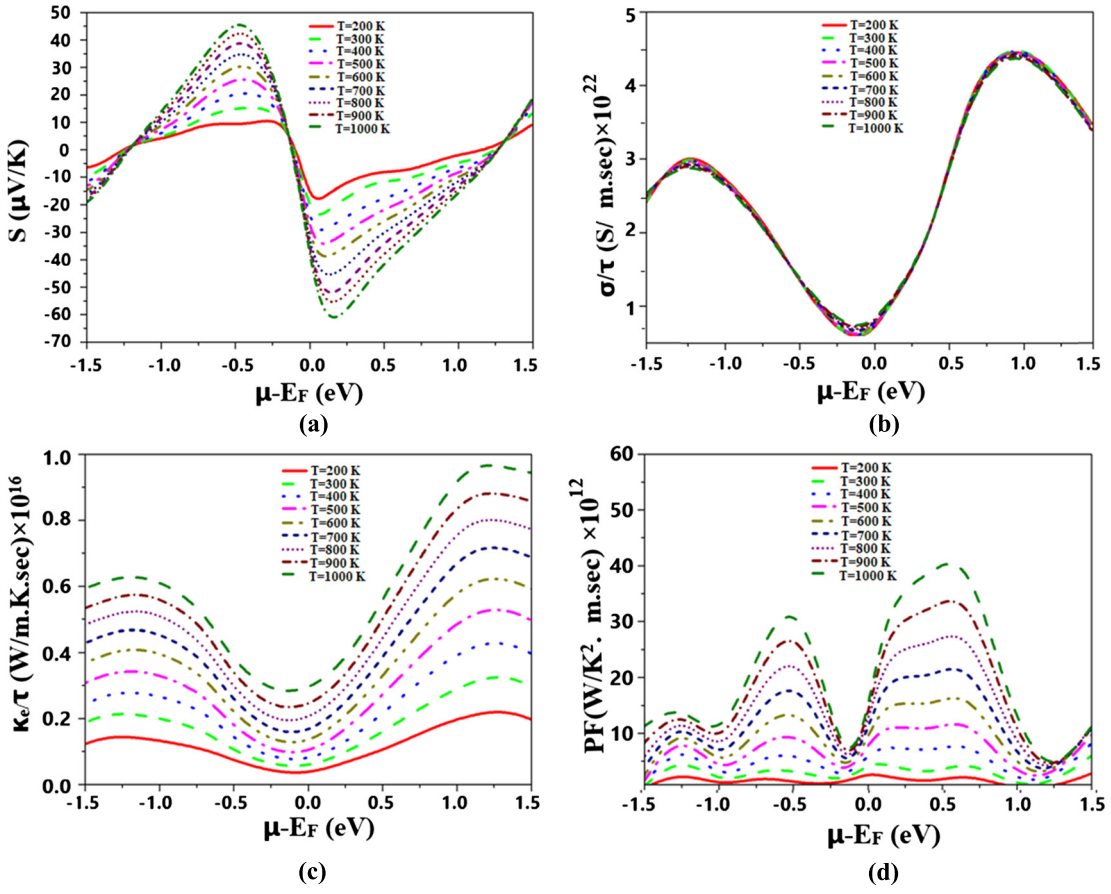

Fig. 5. Variation of (a) Seebeck Coefficient (b) electrical conductivity (c) electronic thermal conductivity and (d) Power Factor as a function of Chemical Potential for LaBi.

LaBi have n-type behavior which is in consistent with other studies [38,58,60].

The value of Power factor w.r.t relaxation time ($S^2\sigma/\tau$) reflects about the performance of thermoelectric material, and has maximum value 43.37×10^{12} $WK^{-2}m^{-1}sec^{-1}$ as shown in Fig. 5(d). It also shows that the studied material is n-type thermoelectric material.

We have also calculated the doping level dependence of transport coefficients at different values of temperatures (i.e. at 300 K, 600 K, 900 K and 1000 K) as depicted in Fig. 6(a)–(d) to reconfirm the n-type behavior of the resultant materials. The doping level is defined as electrons (negative value) or holes (positive values) per unit cell. In the above Figs, the movement of Fermi level into conduction band shows n-type behavior or negative doping levels whereas positive doping level or p-type behavior is shown by shifting of Fermi level in to valence band. From Fig. 6, it is clear that all the parameters have maximum value in the negative range (−0.68 to 0.0) of doping level (N), which confirms the n-type behavior of LaBi, these results are in accordance with the similar predicted compound LaP [36]. The n-type doping yields large values of transport coefficients as compared to that of the p-type.

The variations of thermoelectric properties w.r.t temperature at a fixed value of chemical potential with and without SOC have been plotted from Fig. 7(a)–(f). As shown in Fig. 7(a), the value

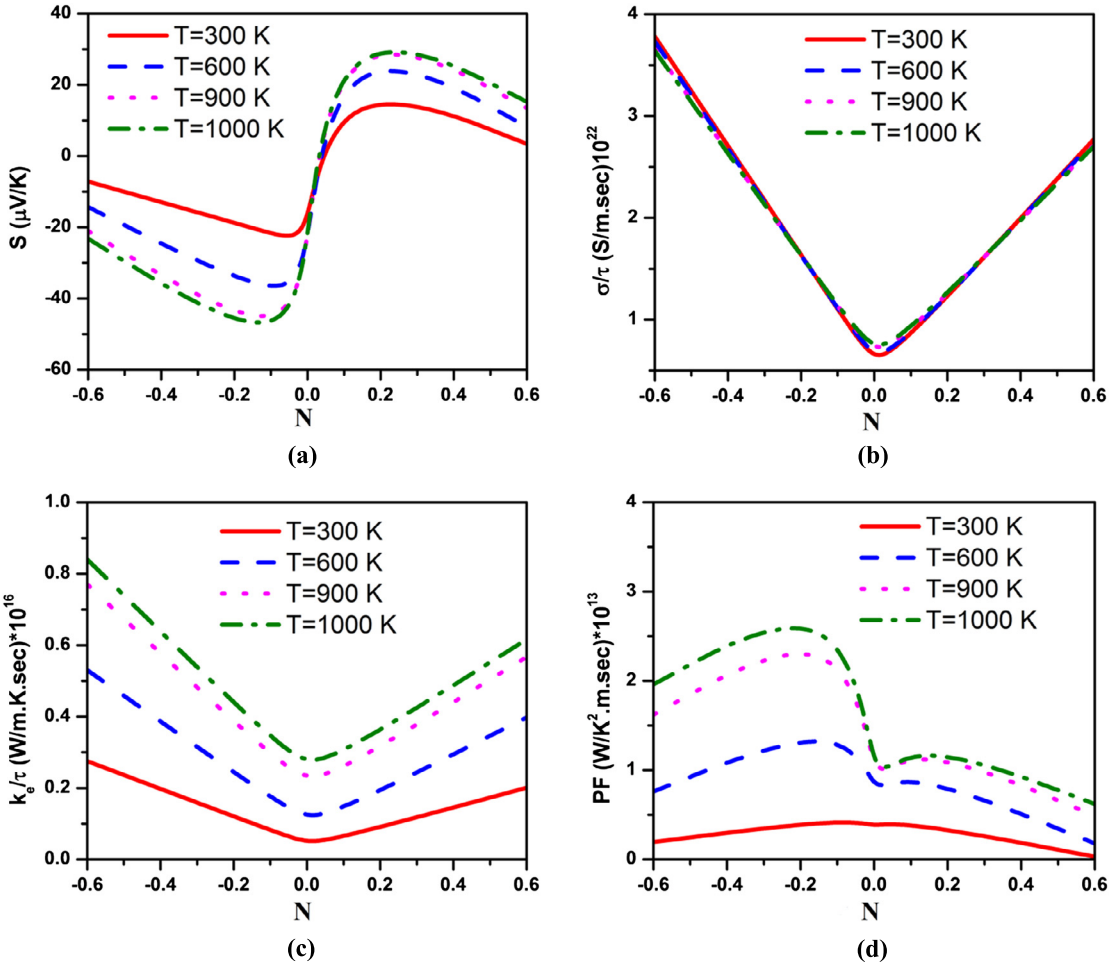

Fig. 6. Variation of (a) Seebeck Coefficient (b) electrical conductivity (c) electronic thermal conductivity and (d) Power Factor as a function of doping level (N) at different values of temperatures for LaBi. Here −ve/+ve doping level refers to electrons (n-type)/hole (p-type) doping.

of Seebeck coefficient ($|S|$) in case of both with/without SOC, increases as temperature increases and attains a maximum value of $-43.85\ \mu VK^{-1}$/and $-40.34\ \mu VK^{-1}$, respectively, at $T = 1000$ K. This enhancement in the value of seebeck coefficient is due to the lifting of band degeneracy by the induction of SOC effect.

In case of metals or degenerate semiconductors, the relation between Seebeck coefficient and temperature is given by:

$$S = \frac{8\pi^2 k_B^2 T}{3qh^2} m^* \left(\frac{\pi}{3n}\right)^{2/3} \tag{8}$$

where k_B, T, q, n, and m^* are the Boltzmann constant, temperature, carrier charge, carrier concentration and effective mass of the carrier, respectively.

Seebeck coefficient measures the induced potential in the material due to the temperature gradient. The electrical conductivity illustrates the contribution of free charge carriers towards electric current; it increases linearly with temperature due to a greater number of thermally excited charge carriers present at high temperature as shown in Fig. 7(b). The value of electrical conductivity with SOC is 0.61×10^{22} $S\,m^{-1}sec^{-1}$ at $T = 300$ K and reaches at 0.75×10^{22} $S\,m^{-1}sec^{-1}$ as temperature rises to 1000 K, whereas without SOC, its value changes from 0.98×10^{22} $S\,m^{-1}sec^{-1}$ to 1.07×10^{22} $S\,m^{-1}sec^{-1}$ at $T = 300$ K and $T = 1000$ K, respectively.

The value of electrical conductivity at room temperature with SOC is very large as compared to theoretically predicted value of topological insulator LaP at room temperature (1.02×10^{22} $S\,m^{-1}sec^{-1}$) [36], half heusler topological semimetal LuPtBi and ScPtBi (0.31×10^{20} S $m^{-1}sec^{-1}$ and 0.45×10^{20} S $m^{-1}sec^{-1}$, respectively) [61]. Our predicted large value of electrical conductivity is due to the semimetallic nature of LaBi which is a crucial factor for the high figure of merit. The power factor (PF) is an important parameter to describe the thermoelectric performance of the material and is strongly dependent on both Seebeck coefficient (S) and electrical conductivity (σ) of the material and its value is larger when we introduce SOC effect. The calculated value of PF with SOC at room temperature is 0.46×10^{13} $WK^{-2}m^{-1}sec^{-1}$ which increases sharply with increase in temperature (Fig. 7(c)), and reaches the value 1.34×10^{12} $WK^{-2}m^{-1}sec^{-1}$ at $T = 1000$ K. Our predicted value of PF at room temperature (0.46×10^{13} $WK^{-2}m^{-1}sec^{-1}$) is very large as compared to Weyl semimetal TaAs (0.53×10^{12} $WK^{-2}m^{-1}sec^{-1}$) [38] and topological insulator LaP (0.4×10^{12} $WK^{-2}m^{-1}sec^{-1}$) [36].

The electronic thermal conductivity (k_e/τ), which tells about heat conduction by electrons increases with increase in temperature as shown in Fig. 7(d). It follows the same trend as that of electrical conductivity defined by Wiedemann-Franz law: $k_e = L\sigma T$, where L is the Lorenz number. Our calculated value of k_e/τ for SOC case is 0.49×10^{15} $W\,m^{-1}K^{-1}sec^{-1}$ at $T = 300$ K, which is better than the value of k_e/τ for LaP ($\sim 0.83\times10^{15}$ $W\,m^{-1}K^{-1}sec^{-1}$) [36] at $T = 300$ K, as low value is beneficial for high ZT. The value of k_e/τ is larger in the case of without SOC calculations as the electrical conductivity is larger.

The lattice thermal conductivity (k_l) also plays an important role in the TE materials as it measures the contribution of phonons

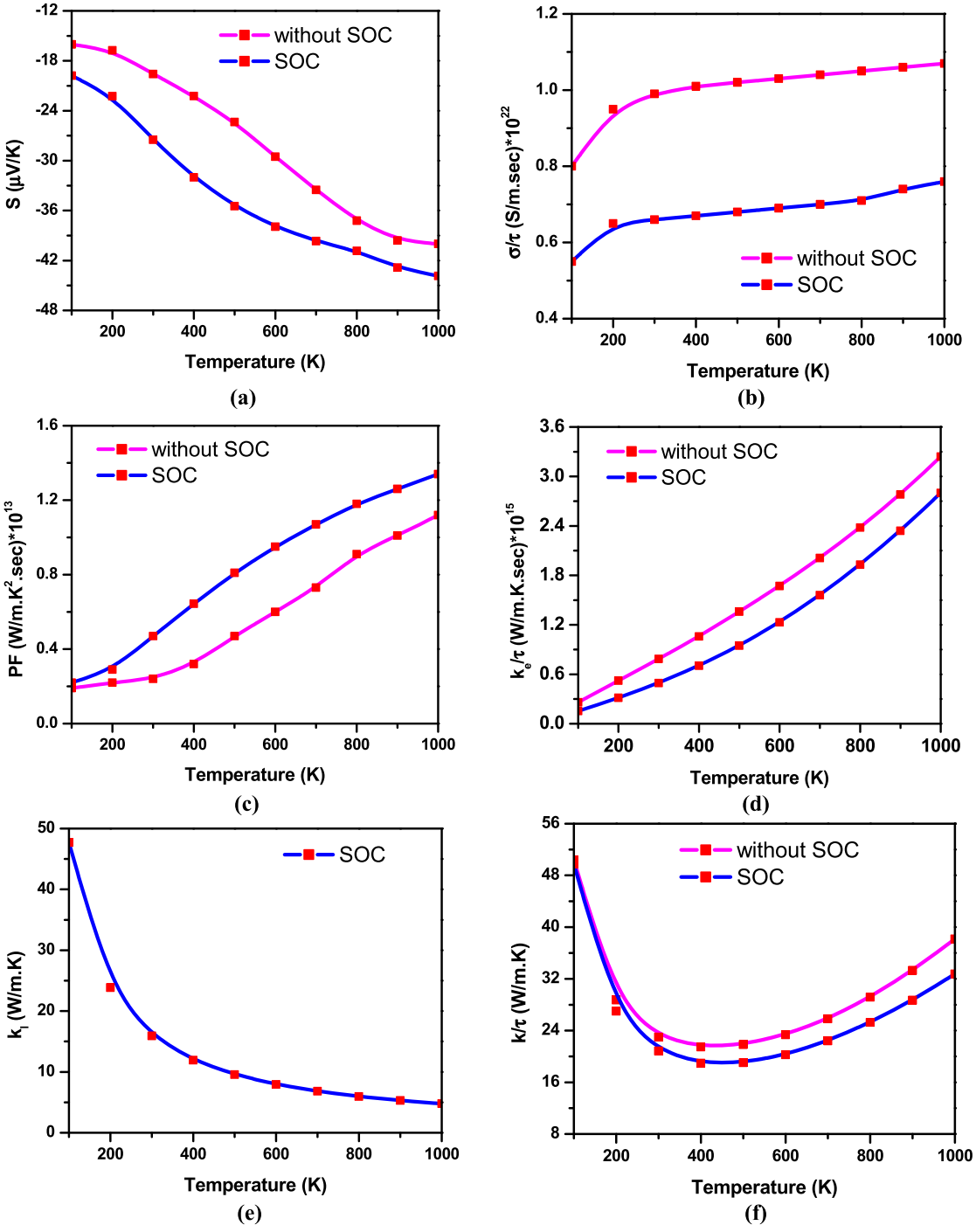

Fig. 7. Variation of (a) Seebeck Coefficient (b) electrical conductivity (c) Power Factor (d) electronic thermal conductivity (e) lattice thermal conductivity (f) Total thermal conductivity versus Temperature for LaBi.

in total thermal conductivity and could be calculated by using Slack's equation [62]:

$$k_l = \frac{AM\delta\theta_D^3}{\gamma^2 n^{2/3} T} \tag{9}$$

where M is the average atomic weight, δ^3 is the average volume of mass equivalent to one atom in the primitive unit cell, θ_D is debye temperature, T is absolute temperature, n is the number of atoms per unit cell and γ is Grünesian parameter. The value of Debye temperature (θ_D) is 208.35 K. The anharmonicity of the material and phonon-phonon scattering are determined by Grünesian parameter (γ) as listed in Table 1. This parameter is related with Poisson's ratio (v) and is calculated by using the following expression:

$$\gamma = \frac{3(1+v)}{2(2-3v)} \tag{10}$$

Large value of γ indicates more phonon scattering, which in turn leads to the small value of lattice thermal conductivity. The coefficient A which depends upon γ [63] is given as:

$$A = \frac{2.43 \times 10^{-8}}{[1 - (0.514\gamma^{-1}) + (0.288\gamma^{-2})]} \tag{11}$$

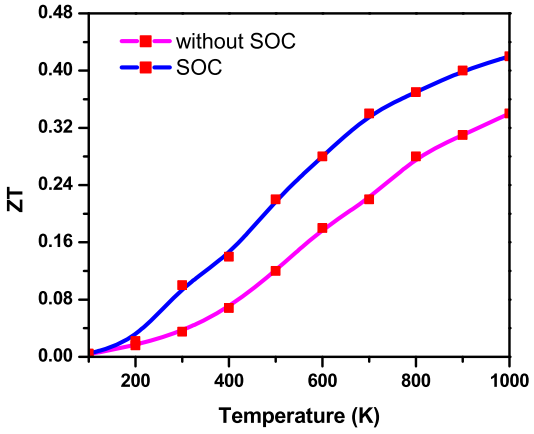

Fig. 8. Figure of merit (ZT) of LaBi as a function of temperature.

The calculated value of lattice thermal conductivity at T =300 K is 15.90 $\mathrm{W\,m^{-1}K^{-1}}$ as observed in Fig. 7(e). We discover that it decreases to a minimum value of 4.20 $\mathrm{W\,m^{-1}K^{-1}}$ at T =1000 K. This is due to the reason that at high temperature, the frequency of lattice vibrations in a solid increase. This large phonon scattering is responsible for the reduced thermal conductivity of the solid. Our predicted value of lattice thermal conductivity of LaBi at room temperature is low as compared to other known efficient thermoelectric materials such as topological semimetals like ZrTe [37], half-Heusler TaIrSn [64], HfRhSb [65] etc., which is an important factor to obtain large figure of merit. The value of lattice thermal conductivity remains same with and without SOC as it depends on the parameters such as average atomic weight, number of atoms per unit cell, Debye temperature etc. which are independent of SOC as depicted by Eq. (9) and shown in Fig. 7(e). The variation of total thermal conductivity (k) with temperature, which includes both electronic thermal conductivity (k_e) as well as lattice thermal conductivity, with temperature is shown in Fig. 6(f). The decrease in total thermal conductivity with temperature is due to the reason that at high temperatures, the component of electronic thermal conductivity dominates over lattice thermal conductivity, which is similar to the case of Dirac semimetal Cd_2As_3 [39] and topological semimetal ZrTe [37].

The efficiency of the TE material is characterized by the dimensionless figure of merit (ZT), which is further related to the transport parameters such as $|S|$, σ and thermal conductivity and can be calculated by the following equation:

$$\mathrm{ZT} = \frac{(\sigma/\tau)S^2T}{(k_e/\tau)+k_l} \tag{12}$$

where ZT directly depends on electrical conductivity and Seebeck coefficient and inversely on thermal conductivity. In BoltzTraP code the relaxation time is unknown, therefore, its value is taken as 10^{-14} sec [61]. We have also compared the ZT value with and without SOC as shown in Fig. 8 and the value of ZT is slightly larger when we introduce SOC effect.

The calculated value of ZT with SOC at T =300 K is 0.10 which is almost comparable to the ZT value of topological insulator LaP (0.11) [36]. It increases with increase in temperature and reaches to a maximum value of 0.42 at T =1000 K which is larger than the value of ZT for half Heusler topological semimetal ScPtBi (0.3) and YPtBi (0.4) [61]. This increase in value of ZT is mainly due to two factors; first one is the increase in PF with increase in temperature and second is the decrease in value of lattice thermal conductivity with increase in temperature. It indicates that the value of ZT can be improved by increasing the temperature, and the studied material LaBi may be a promising thermoelectric material for high temperature applications.

4. Conclusions

The structural, electronic, mechanical and thermoelectric properties of LaBi have been studied using first-principles calculations combined with Boltzmann transport theory. The calculated lattice parameter of LaBi is in agreement with the available theoretical and experimental data. The calculated value of lattice thermal conductivity at room temperature is found to be 15.91 $\mathrm{W\,m^{-1}K^{-1}}$ which decreases with increase in temperature and reaches a minimum value at T =1000 K. The value of power factor increases with increase in temperature and reaches to a maximum value of 1.34×10^{13} $\mathrm{WK^{-2}m^{-1}sec^{-1}}$ at T =1000 K which is larger than that of recently predicted Topological material (LaP). The large value of PF and low value of lattice thermal conductivity strongly suggest that LaBi may act as efficient thermoelectric material. The figure of merit also shows increasing behavior with temperature and attains a maximum value of 0.42 as temperature is raised from 200 to 1000 K. All these findings clearly show that the studied material may be an efficient thermoelectric material for high temperature applications.

CRediT authorship contribution statement

Conception and design of study: Nisha, Hardev S. Saini, Sunita Srivastava and Manish K. Kashyap, acquisition of data: Nisha, Hardev S. Saini, Narender Kumar, Satyender Singhmar, Jyoti Thakur, Ali H. Reshak, analysis and/or interpretation of data: Nisha, Hardev S. Saini, Sunita Srivastava and Manish K. Kashyap, Ali H. Reshak.

Drafting the manuscript: Nisha, Hardev S. Saini, Sunita Srivastava and Manish K. Kashyap, Ali H. Reshak, revising the manuscript critically for important intellectual content: Nisha, Hardev S. Saini, Narender Kumar, Satyender Singhmar, Jyoti Thakur, Sunita Srivastava and Manish K. Kashyap, Ali H. Reshak.

Approval of the version of the manuscript to be published (the names of all authors must be listed): Nisha, Hardev S. Saini, Narender Kumar, Satyender Singhmar, Jyoti Thakur, Sunita Srivastava and Manish K. Kashyap, Ali H. Reshak.

Declaration of competing interest

The authors declare that they have no known competing financial interests or personal relationships that could have appeared to influence the work reported in this paper.

Acknowledgement

One of the authors, H.S. Saini acknowledge the financial support from GJUS&T, Hisar in the form of a minor research project vide grant no. Acad. /AC-III/F-90/2019/5139-48.

References

[1] S.B. Riffat, X. Ma, Appl. Therm. Eng. 23 (2003) 913.
[2] M. Zebarjadi, K. Esfarjani, M.S. Dresselhaus, Z.F. Ren, G. Chen, Energy Environ. Sci. 5 (2012) 5147.
[3] G.J. Snyder, E.S. Toberer, Nat. Mater. 7 (2008) 105.
[4] J.R. Salvador, J.Y. Cho, Z. Ye, J.E. Moczygemba, A.J. Thompson, J.W. Sharp, J.D. Koenig, R. Maloney, T. Thompson, J. Sakamoto, H. Wang, A.A. Wereszczak, Phys. Chem. Chem. Phys. 16 (2014) 12510.
[5] A. Saramat, G. Svensson, A.E. Palmavist, C. Stiewe, E. Mueller, D. Platzek, J. Appl. Phys. 99 (2006) 023708.
[6] A.F. May, J.P. Fleurial, G.J. Snyder, Phys. Rev. B 78 (2008) 125205.
[7] C.G. Fu, S.Q. Bai, Y.T. Liu, Y.S. Tang, L.D. Chen, X.B. Zhao, T.J. Zhu, Nat. Commun. 6 (2015) 8144.
[8] B. Yan, S.C. Zhang, Rep. Prog. Phys. 75 (2012) 096501.
[9] Nisha, K. Kaur, J. Thakur, M.K. Kashyap, H.S. Saini, AIP Conf. Proc. 2115 (2018) 030426.
[10] H. Zhang, C.X. Liu, X.L. Qi, X. Dai, Z. Fang, S.C. Zhang, Nat. Phys. 5 (2009) 438.

[11] D. Hsieh, Y. Xia, D. Qian, L. Wray, F. Meier, J.H. Dil, J. Osterwalder, L. Patthey, A.V. Fedorov, H. Lin, A. Bansil, D. Grauer, Y.S. Hor, R.J. Cava, M.J. Hasan, Phys. Rev. Lett. 103 (2009) 146401.
[12] T.H. Hsieh, H. Lin, J. Liu, W. Duan, A. Bansil, L. Fu, Nat. Commun. 3 (2012) 982.
[13] X.L. Qi, S.C. Zhang, Phys. Today 63 (2009) 33.
[14] J.E. Moore, Nature 464 (2010) 194.
[15] N. Xu, Y. Xu, J. Zhu, npj Quantum Mater. 2 (1) (2017) 1.
[16] D. Baldomir, D. Failde, Sci. Rep. 9 (2019) 6324.
[17] D. Kong, Y. Cui, Nat. Chem. 3 (2011) 845.
[18] A.A. Burkov, Nat. Mater. 15 (2016) 1145.
[19] H. Li, H. He, H.Z. Lu, H. Zhang, H. Liu, R. Ma, Z. Fan, S.Q. Shen, J. Wang, Nat. Commun. 7 (2011) 10301.
[20] Z. Wang, Y. Sun, X.-Q. Chen, C. Franchini, G. Xu, H. Weng, X. Dai, Z. Fang, Phys. Rev. B 85 (2012) 195320.
[21] H. Weng, C. Fang, Z. Fang, B.A. Bernevig, X. Dai, Phys. Rev. X 5 (2015) 011029.
[22] A.A. Burkov, M.D. Hook, L. Balents, Phys. Rev. B 84 (2011) 235126.
[23] G.B. Halasz, L. Balents, Phys. Rev. B 85 (2012) 035103.
[24] S.S. Sun, Q. Wang, P.J. Guo, K. Liu, H.C. Lei, New J. Phys. 18 (2016) 082002.
[25] N. Kumar, C. Shekhar, I. Leemakers, O. Young, U. Zeitter, B.H. Yan, C. Felser, Phys. Rev. B 93 (2016) 241106.
[26] C.H. Li, D. Broido, Phys. Rev. B 95 (2017) 205203.
[27] Y.O. Ciftci, K. Colakoglu, E. Deligoz, J. Phys. Condens. Matter 20 (2008) 345202.
[28] R. Singha, B. Satpati, P. Mandal, Sci. Rep. 7 (2017) 6321.
[29] C. Stampfl, W. Mannstadt, R. Asahi, A.J. Freeman, Phys. Rev. B 63 (2001) 155106.
[30] J. Nayak, Shu-Chun Wu, N. Kumar, C. Shekhar, S. Singh, J. Fink, Emile E.D. Rienks, G.H. Fecher, Stuart S.P. Parkin, B. Yan, Claudia Felser, Nat. Commun. 8 (2017) 13942.
[31] R. Lou, B.B. Fu, Q.N. Xu, P.J. Guo, L.Y. Kong, L.K. Zeng, J.Z. Ma, P. Richard, C. Fang, Y.B. Huang, S.S. Sun, Q. Wang, L. Wang, Y.G. Shi, H.C. Lei, K. Liu, H.M. Weng, T. Qian, H. Ding, S.C. Wang, Phys. Rev. B 95 (2017) 115140.
[32] X.H. Niu, D.F. Xu, Y.H. Bai, Q. Song, X.P. Shen, B.P. Xie, Z. Sun, Y.B. Huang, D.C. Peets, D.L. Feng, Phys. Rev. B 94 (2016) 165163.
[33] B. Feng, J. Cao, M. Yang, Y. Feng, S. Wu, B. Fu, M. Arita, K. Miyamoto, S. He, K. Shimada, Y. Shi, T. Okuda, Y. Yao, Phys. Rev. B 97 (2018) 155153.
[34] U. Dey, M. Chakraborty, A. Taraphder, S. Tewari, Sci. Rep. 8 (2018) 14867.
[35] U. Dey, J. Phys. Condens. Matter 30 (2018) 205501.
[36] Y. Zhou, W.L. Tao, Z.Y. Zeng, X.R. Chen, Q.F. Chen, J. Appl. Phys. 125 (2019) 045107.
[37] S.D. Guo, Y.H. Wang, W.L. Lu, New J. Phys. 19 (2017) 113044.
[38] B. Peng, H. Zhang, H. Shao, H. Lu, D.W. Zhang, H. Zhu, Nano Energy 30 (2016) 225.
[39] Zhou, C. Zhang, H. Zhang, F. Xiu, Z. Yang, Inorg. Chem. Front. 3 (2016) 1637.
[40] U. Stockert, R.P. Dos Reis, M.O. Ajeesh, S.J. Watzman, M. Schmidt, C. Shekhar, J.P. Heremans, C. Felser, M. Baenitz, M. Nicklas, J. Phys. Condens. Matter 29 (2017) 325701.
[41] S.D. Guo, J. Phys. Condens. Matter 29 (2017) 435704.
[42] K. Schwarz, P. Blaha, G.K.H. Madsen, Comput. Phys. Commun. 147 (2002) 71.
[43] F. Tran, P. Blaha, Phys. Rev. Lett. 102 (2009) 226401.
[44] M. Jamal, M. Bilal, I. Ahmad, S.J. Asadabadi, J. Alloys Compd. 739 (2018) 569.
[45] G.K.H. Madsen, D.J. Singh, BoltzTraP, Comput. Phys. Commun. 175 (2006) 67.
[46] A. Otero-de-la-Roza, D. Abbasi-Perez, V. Luana, Comput. Phys. Commun. 182 (2011) 2232.
[47] A. Togo, I. Tanaka, Scr. Mater. 108 (2015) 1.
[48] A. Togo, I. Tanaka, Phys. Rev. B 87 (2013) 184104.
[49] G. Vaitheeswaran, V. Kanchana, M. Rajagopalan, Physica B 315 (2002) 64.
[50] J.Y. Wang, Y.C. Zhou, Phys. Rev. B 69 (2004) 214111.
[51] M. Born, K. Huang, Dynamical Theory of Crystal Lattices, Claendron, Oxford, 1954.
[52] A. Reuss, Z. Angew, Math. Mech. 9 (1929) 49.
[53] W. Voigt, Textbook of Crystal Physics, 1st ed., B.G. Teubner, Leipzig, Berlin, 1946.
[54] R. Hill, Proc. Phys. Soc. A 65 (1952) 349.
[55] M.A. Blanco, E. Francisco, V. Luana, Comput. Phys. Commun. 158 (2004) 57.
[56] H. Fu, X. Li, W. Liu, Y. Ma, T. Gao, X. Hong, Intermetallics 67 (2011) 1959.
[57] S.F. Pugh, XCII, Philos. Mag. 45 (1954) 823.
[58] J.Y. Wang, Y.C. Zhou, Z.J. Lin, Acta Mater. 55 (2007) 6019.
[59] E. Deligoz, K. Colakoglu, Y.O. Ciftci, H. Ozisik, J. Phys. Condens. Matter 19 (2007) 436204.
[60] K. Kaur, J. Kaur, J. Alloys Compd. 715 (2017) 297.
[61] K. Kaur, S. Dhiman, R. Kumar, Phys. Lett. A 381 (4) (2017) 339.
[62] D.T. Morelli, G.A. Slack, High Lattice Thermal Conductivity of Solids, Springer, New York, USA, 2006.
[63] C.L. Julian, Phys. Rev. 137 (1965) 128.
[64] K. Kaur, R. Kumar, Phys. Lett. A 381 (2017) 3760.
[65] K. Kaur, R. Kumar, D.P. Rai, J. Alloys Compd. 763 (2018) 1018.